34^{th} *Scandinavian Symposium on Physical Acoustics,* 30^{th} *January -* 2^{nd} *February 2011*

Finite element analysis of acoustic beam interactions with a plate at normal incidence. Comparison with a 3D angular spectrum method and measurements.

Magne Aanes[a,c,*], Kjetil Daae Lohne[b,c], Per Lunde[a,b,c], Magne Vestrheim[a,c]

[a] *University of Bergen, Department of Physics and Technology, Postboks 7803, N-5020 BERGEN, Norway*
[b] *Christian Michelsen Research AS (CMR), P.O. Box 6031 Postterminalen, N-5892 BERGEN, Norway*
[c] *The Michelsen Centre for Industrial Measurement Science and Technology*

Abstract

The use of the finite element method (FEM) for studying the interactions of an acoustic beam with an elastic steel plate is discussed, in comparison with a 3D angular spectrum method (ASM) and measurements. The on-axis sound pressure generated by a circular piston source at normal incidence through a steel plate is investigated. In the 3D ASM, aswell as in the measurements, pulses are utilized in order to propagate an incident wave towards the steel plate. In these methods the transmitted on-axis pressure is normalized to the incident on-axis pressure at the upper surface of the steel plate in order to calculate the transmitted frequency spectrum. Using a frequency domain 3D FEM continues waves are used instead of pulses, creating a standing wave pattern between the piston source and the steel plate. The transmitted on-axis pressure calculated using the 3D FEM contains therefore effects of this standing wave pattern. In an attempt to reduce these effects in the transmitted frequency spectrum, the total on-axis pressure at the upper surface of the steel plate is used instead of the incident on-axis pressure. In order to compare the 3D FEM to the 3D ASM and measurements, the relationship between these two on-axis pressures must be identified.

1. Introduction

The study of an acoustic beam interacting with an elastic steel plate or a pipe wall is important in many applications such as non-invasive ultrasonic flow metering [1, 2], NDT(non-destructive-testing) [3, 4, 5, 6, 7, 8, 9, 10, 11], detection of wax/hydrate-formation [12, 13, 14, 15] and transducer technology. Such applications require a comprehensive understanding, control and optimization of the generation, transmission and reception of sound through plates/pipes and the surrounding fluid. Similar studies using plane wave theory [16, 17, 18], two dimensional cartesian (2D) angular spectrum methods (ASM) [19, 20, 21] and three dimensional (3D) angular spectrum methods (ASM) [10, 11, 4] have been made. One limitation in such models is how the imposed sound field is generated. In the plane wave theory the sound field is generated by a plane wave with a certain angle of incidence. Using a 2D ASM, the directivity of the imposed sound field will not be correctly taken into account. In many applications a more realistic and accurate description of the sound field radiated from a real source is needed. The 3D ASM can account for a directive beam, either by implementing a simplified one, e.g. the sound field from a circular piston source, or by importing a sound field from measurements or other simulation models. The transducer construction and properties are of critical importance for excitation of the desired waveguide. Therefore the transmitting and receiving transducers should be accounted for in the modeling, for a more complete description of the signal chain. The finite element method (FEM) can model a full piezoelectric transducer and its directive beam. In the present work the feasibility of the 3D FEM for discribing the interaction of an acoustic beam with a steel plate at

*Corresponding author
Email address: `Magne.Aanes@ift.uib.no` (Magne Aanes)

normal incidence is studied, in comparison with a 3D ASM and measurements. Challenges of applying the 3D FEM, regarding the handling of unbounded media, in addition to issues applying a frequency domain FEM will be discussed.

The 3D ASM used here for comparison [4, 6] uses an uniformly vibrating circular piston source mounted in a rigid baffle of infinite extent for the generation of sound. In the 3D ASM, aswell as in the measurements, pulses are utilized in order to propagate an incident wave towards the steel plate. In order to compare the 3D FEM with the 3D ASM the acoustic beam is also generated by a circular piston source in the 3D FEM. Using a frequency domain 3D FEM continues waves are used instead of pulses, creating a standing wave pattern between the piston source and the steel plate. A rigid baffle situated on the sides of the circular piston will therefore increase the unwanted standing wave pattern considerably. For that reason no rigid baffle is included in the FE simulations, minimizing the standing wave pattern, and the uniformly vibrating circular piston source is immersed in water without any baffle. Fig. 1 illustrates an acoustic beam generated by a unbaffled circular piston source and interacting at normal incidence with a steel plate immersed in water. At normal incidence an 2D axisymmetric coordinate system (r, z) can be used to describe a 3D beam, reducing the number of finite elements relative to using a full 3D coordinate system. The steel plate is located at a distance of 270 mm from the circular piston source. The transmitted on-axis pressure at a distance of 100 mm below the lower surface of the steel plate is calculated, see '*' in Fig. 1. This on-axis pressure is normalized to the on-axis pressure at the upper surface of the steel plate, see 'X' in Fig. 1 in order to calculate the transmitted frequency spectrum. In the 3D ASM and in the measurements the transmitted on-axis pressure is normalized to the incident on-axis pressure. The transmitted on-axis pressure calculated using the 3D FEM contains effects of the standing wave pattern. In an attempt to reduce these effects, the total on-axis pressure is used, i.e. the on-axis pressure when the plate is present, instead of the incident on-axis pressure. In order to compare the 3D FEM to the 3D ASM and measurements, the relationship between these on-axis pressures must be identified.

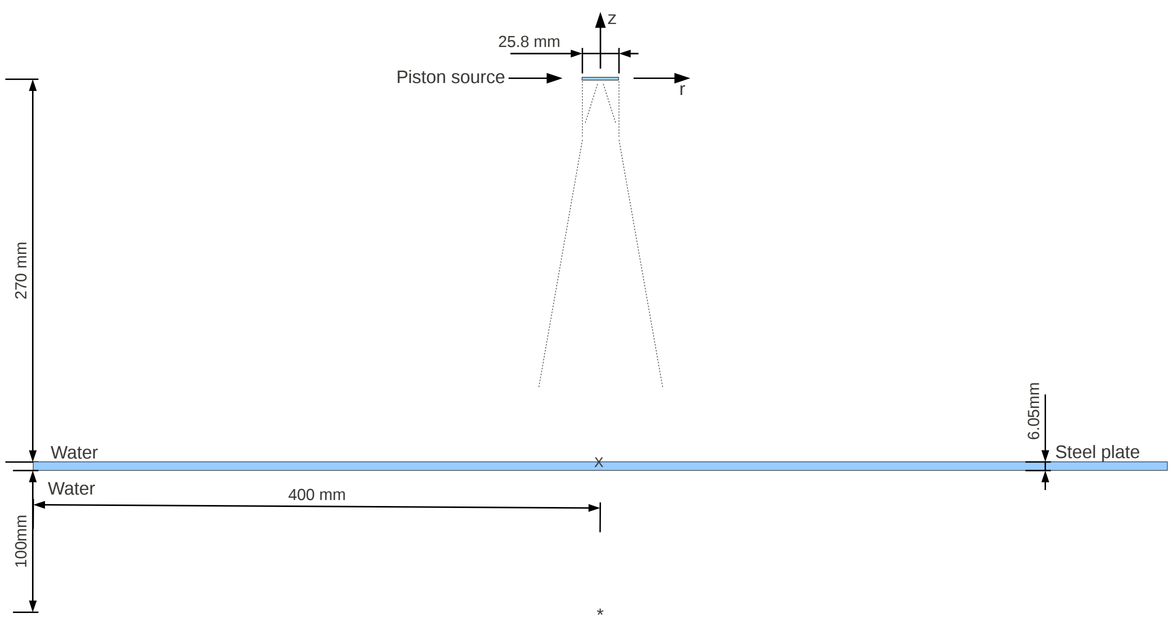

FIG 1. An illustration of an acoustic beam, generated by a unbaffled uniformly vibrating circular piston source, interacting with a 6.05 mm thick water immersed steel plate at normal incidence. The distance between the piston source and the upper surface of the steel plate is 270 mm. The transmitted on-axis pressure is calculated at a distance of 100 mm below the steel plate, at '*'. This pressure is normalized by the on-axis pressure at the upper surface of the steel plate at 'X' for the calculation of the transmitted frequency spectrum.

2. Theory

2.1. Leaky Lamb waves for an elastic plate (plane waves)

A traditional way of studying guided waves in an elastic isotropic plate of infinite extent is using the leaky Lamb wave theory [22]. Fig. 2 gives a schmatic illustration of leaky wave propagation in an infinite elastic plate of thickness $2L$, immersed in a fluid (semi-infinite half spaces above and beneath the plate). The arrows above the plate shows the directions of the incident and reflected compressional waves with a velocity of c_l. The density of the fluid is ρ_f. Inside the plate, waves with shear velocity c_S and compressional velocity c_L are established respectively, where ρ_s is the density of the plate. Beneath the plate a compressional wave is transmitted into the fluid.

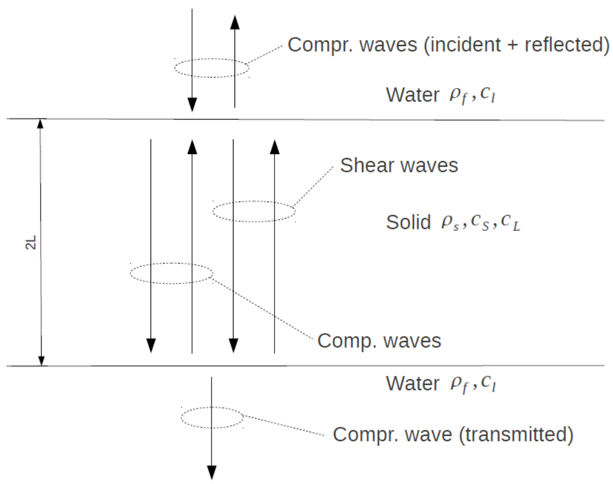

FIG 2. Schematic illustration of leaky wave propagation in an infinite long and wide solid plate with a thickness $2L$. The solid plate is immersed in two semi-infinite half spaces of water. The arrows indicate the direction of the waves established by the incident compressional wave. Schematic representation for an oblique angle of incidence.

For certain frequencies standing compressional and shear waves are present across the thickness of the plate [4, 22]. These frequencies occur where the phase velocity for the generated Lamb waves of the solid plate approaches infinity [23]. The frequencies can be calculated from the dispersion equations for the symmetrical and antisymmetrical leaky Lamb modes by letting the horizontal wavenumber η approach zero [4, 5]. Since the ratio between the density of the steel plate and the water is high, this condition is almost equivalent to using a normal incidence plane wave from the fluid to generate these resonances in the steel plate. The critical frequencies $f_{L,n}$ and $f_{S,n}$ for thickness extensional (TE) and thickness shear (TS) modes in the plate respectively are given as [4, 5]

$$f_{L,n} = \frac{c_L n}{4L}, \tag{1}$$

$$f_{S,n} = \frac{c_S m}{4L,}, \tag{2}$$

where n, $m = 1,2,3,...$ These frequencies can be used to determine the compressional c_L and shear velocity c_S of the steel plate by measuring the frequencies where a maximum or a minimum of the transmitted pressure is calculated [4].

2.2. 3D Angular spectrum method (ASM)

The angular spectrum method (ASM) models the propagation of a beam by representing the wave pattern as an integration of plane waves. The method propagates a known pressure field at a reference plane from that plane to other parallel planes in the frequency-wavenumber domain using the spatial 2D Fourier transform [4, 6]. This calculation of the pressure field includes diffraction and reflection/transmission through the different planes employed. The 3D ASM used in this paper is described in [4] and uses the far field solution of the sound field radiated by an uniformly vibrating circular piston source mounted in a rigid baffle of infinite extent, for the known pressure field at the reference plane. The piston source can have an oblique angle of incidence towards the steel plate immersed in water as investigated in [4, 6], but in this work a comparison with normal incidence results from [4, 6] are used. This method can then calculate the incident or total (incident + reflected) on-axis pressure at the upper surface of the steel plate, and the transmitted pressure at a certain distance below the lower surface of the steel plate, making it possible to calculate the transmitted frequency spectrum and time domain signals. Further details on the 3D ASM is given in [4, 6].

2.3. 3D Finite element method (FEM)

The 3D finite element (FE) implementation used here is FEMP 5 [24, 25, 26], which is a frequency domain implementation. For axisymmetric simulations this implementation uses 8 node isoparametric elements for both the fluid and elastic finite elements [24]. For the handling of an infinite fluid region perfectly matched layers (PMLs) [26, 27, 28, 29] are used here. The PML method can be interpreted as a coordinate stretching in the frequency domain through a complex change of variables. In the direction x, where x denotes either r or z, the coordinate transformation is

$$\frac{\partial}{\partial x} \rightarrow \frac{\partial}{\partial x^{‘}} = \frac{1}{\gamma_x}\frac{\partial}{\partial x}, \tag{3}$$

where γ_x is defined by

$$\gamma_x = 1 + \frac{i}{\omega}\sigma_x(x) \qquad , x \geq x^* \tag{4}$$

$$\gamma_x = 1 \qquad , x < x^*. \tag{5}$$

The damping function σ used in this paper is an 'optimal' damping function introduced by [28]

$$\sigma = \frac{c_l}{x^* - x}, \tag{6}$$

where x^* is truncation of the normal fluid region in the x direction, and c_f is the compressional sound velocity in the fluid. In the FE implementation used, there is no possibility for having frequency dependent mass- and stiffness matrices [26]. In order to get the frequency dependency out of Eq. 4 a σ^* is defined as $\sigma^* = \sigma\omega/\omega_0$ [26] and used for σ_x, see Eq. 7.

$$\gamma_x = 1 + \frac{i}{\omega_0}\sigma(x) \qquad , x \geq x^* \tag{7}$$

For modelling an infinite elastic medium without end reflections (such as for the plate) a "decreasing Q_M" method [12] has been employed here since for the current version of FEMP 5, PML for elastic regions [26] have not been implemented yet. This "decreasing Q_M" method reduce the loss factor Q_M exponentially inside a region of an elastic medium to approximately zero, thus reducing the reflections from the endfaces of that region.

2.4. *Transmitted frequency spectrum (TFS) for the 3D ASM and the 3D FEM*

The "transmitted frequency spectrum" (TFS) is here defined as

$$\mathrm{TFS}_0^{\mathrm{MODEL}} = \frac{p^{\mathrm{MODEL}}}{p_0^{\mathrm{MODEL}}}, \tag{8}$$

where p^{MODEL} is the transmitted on-axis pressure at a distance of 100 mm below the steel plate for the $^{\mathrm{MODEL}}$ applied, either 3D FEM or 3D ASM, see '*' in Fig. 1. The p_0^{MODEL} is the on-axis pressure in the fluid at the upper surface of the steel plate, see 'X' in Fig. 1.

In this paper two on-axis pressures p_0, denoted p_{inc} and p_{tot}, see Eq. 9, are used to normalize the transmitted on-axis pressure p^{MODEL} for both the 3D ASM and the 3D FEM. These normalization methods are denoted normalization method no. 1 ('norm 1') and normalization method no. 2 ('norm 2') respectively as

$$p_0 = \begin{Bmatrix} p_{inc}^{\mathrm{MODEL}}, \text{ for normalization method no. 1} \\ p_{tot}^{\mathrm{MODEL}}, \text{ for normalization method no. 2} \end{Bmatrix} \tag{9}$$

The incident on-axis pressure p_{inc} in the water at the upper surface of the plate when the plate is absent is used for p_0 in normalization method no. 1, in order to compare the simulations to the measurements made by [4, 6]. Using the 3D FEM, standing waves appear between the unbaffled circular piston source and the upper surface of the plate. In an attempt to reduce the effects the standing wave pattern will have on the transmitted frequency spectrum the total on-axis pressure p_{tot} in the water at the upper surface of the plate when the plate is present is used for p_0 in normalization method no. 2.

For the 3D ASM the transmitted frequency spectra with normalization method no. 1 and no. 2 are expressed respectively as

$$\mathrm{TFS}_{inc}^{\mathrm{ASM}} = \frac{p^{\mathrm{ASM}}}{p_{inc}^{\mathrm{ASM}}}, \qquad \mathrm{TFS}_{tot}^{\mathrm{ASM}} = \frac{p^{\mathrm{ASM}}}{p_{tot}^{\mathrm{ASM}}}. \tag{10}$$

For the 3D FEM the transmitted frequency spectra with normalization method no. 1 and no. 2 are expressed respectively as

$$\mathrm{TFS}_{inc}^{\mathrm{FEM,sw}} = \frac{p^{\mathrm{FEM,sw}}}{p_{inc}^{\mathrm{FEM}}}, \qquad \mathrm{TFS}_{tot}^{\mathrm{FEM}} = \frac{p^{\mathrm{FEM,sw}}}{p_{tot}^{\mathrm{FEM,sw}}}, \tag{11}$$

where the superscript $^{\mathrm{sw}}$ denotes that the effects of the standing waves are present. Here the effects of the standing wave pattern are assumed to be the same for the transmitted $p^{\mathrm{FEM,sw}}$ and total on-axis pressure $p_{tot}^{\mathrm{FEM,sw}}$, so that the effects of the standing wave pattern is removed in the $\mathrm{TFS}_{tot}^{\mathrm{FEM}}$, written then without the superscript $^{\mathrm{sw}}$. Mark that the incident on-axis pressure p_{inc}^{FEM} and p_{inc}^{ASM} are not the same, since an unbaffled piston source is used in the 3D FEM in contrast to a baffled piston source the 3D ASM, see more in Section 5.3. Mark also that the pressure $p_{tot}^{\mathrm{FEM,sw}}$ includes the standing wave pattern between the piston source and the plate, in constrast to the p_{tot}^{ASM} which includes the imposed incident wave and the reflected wave at the upper surface of the plate.

In the figures throughout this paper the transmitted on-axis pressure is denoted p, and the on-axis pressure used for the normalization is denoted p_0, regardless of which model and normalization method used. In every case, the model and normalization method used to calculate the TFS is given explicitly, either in the text or in the figure label.

3. Experimental setup

The measurements are described in [4, 5, 6]. A 6.05 mm thick, 500 mm wide and 760 mm long AISI 316L stainless steel plate is immersed in water in a tank with dimensions (150×60×60) cm (length×height×width), see Fig. 3. A Panametrics V301 500 kHz transducer is mounted on the left side of the steel plate at normal incidence towards the steel plate. A Precision Acoustics (PA) 1 mm needle calibrated PVDF probe hydrophone (PA-407) is mounted on the far side of the steel plate, see the sketch in Fig. 3. The distance between the transducer and the steel plate is 270 mm. The transmitted on-axis pressure p^{MEAS} at a distance 100 mm from the right surface of the steel plate is measured by the hydrophone for each frequency in the frequency range of interest. This transmitted pressure is normalized to the incident on-axis pressure p_{inc}^{MEAS} at the front surface of the steel plate when the plate is absent, in order to calculate the $\mathrm{TFS}_{inc}^{\mathrm{MEAS}}$ [4, 6]. The steel plate was therefore removed and the hydrophone was moved to the position of the left surface of the steel plate for the incident on-axis pressure measurements. For more information regarding the measurements refer to [4, 6].

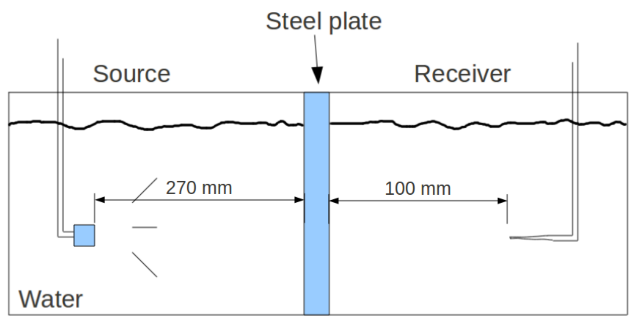

FIG 3. Sketch of the measurement tank with the 6.05 mm thick steel plate immersed in water. A Panametrics V301 500 kHz transducer is mounted on the left hand side of the steel plate, and the transmitted pressure is measured by a PA 1 mm needle hydrophone on the right hand side of the steel plate.

4. Simulations

4.1. Leaky Lamb waves for an elastic plate (plane waves)

The plane wave pressure transmission coefficient T in Eq. 12 is calculated using the leaky Lamb wave theory for a 6.05 mm thick water immersed infinite long steel plate [4, 5].

$$T = \frac{p_t}{p_i}, \tag{12}$$

where the transmitted pressure p_t at the lower surface, see Fig. 2 (right surface in Fig. 3), of the steel plate is normalized to the incident pressure p_i on the upper surface, see Fig. 2 (left surface in Fig. 3), of the steel plate. The material data for the steel plate and the surrounding water are listed in Table. 1.

TABLE 1. Material properties used in the leaky Lamb wave theory [4, 5], the 3D ASM [4, 6] and the 3D FEM.

Material	ρ [kg/m^3]	c_L[m/s]	c_S[m/s]
AISI 316L stainless steel	8000	5780	3050
Water	1000	1483	-

4.2. 3D Angular spectrum method (ASM)

An uniformly vibrating circular and baffled piston source with a radius of 12.9 mm radiating at normal incidence towards a 6.05 mm thick steel plate is used in the 3D ASM [4, 6]. The distance between the piston source and the plate is 270 mm, and the distance between the plate and the receiver is 100 mm, see Fig. 1. The material data for the steel plate and water are given in Table. 1, the same as for the plane wave theory. The transmitted on-axis pressure p^{ASM} at a distance of 100 mm below the steel plate is calculated and normalized to the incident p_{inc}^{ASM} or the total p_{tot}^{ASM} on-axis pressure on the upper surface of the steel plate respectively. The normalization methods are discussed in detail in Section 2.4. For more information of the implementation of the 3D ASM it is refered to [4, 6].

4.3. 3D Finite element method (FEM)

In an axisymmetric coordinate system (r, z) an uniformly vibrating circular piston source with the center of the surface in origo $(0, 0)$, radiates at a certain frequency into the surrounding water. The radius of the piston is 12.9 mm and the thickness is 0.01 mm. The piston has a forced displacement with an amplitude of 1×10^{-6} mm (1 nm) along the z-axis over the entire surface for each simulated frequency. A circular steel plate is present at a distance of $z = -270$ mm from the piston surface, with a radius of $r = 400$ mm. The steel plate thickness is $2L = 6.05$ mm. The circular piston has a normal incidence towards the steel plate, see Fig. 1 for a description. The material data are given in Table. 1, exept the loss factor Q_M for the steel plate. In the leaky Lamb wave theory and the 3D ASM the steel plate is assumed lossless. Since the "decreasing Q_M" method must be used to dampen the outgoing waves in the steel plate a loss factor Q_M for the steel plate must be assumed, and here $Q_M = 100$ has been used. In comparison of the results to the measurements in Section 5 this Q_M may seem a bit low, but was used in order to properly reduce the endface reflections in steel plate for these simulations.

A coarse decimated mesh of the FE simulations is shown in Fig. 4 in order to visualize the implementation of the circular piston source, the steel plate and the fluid PMLs. The element division in this figure is less detailed than the actual simulations. Here fluid perfectly matched layers (PMLs) are used to prevent reflections from the endfaces of the water (blue) regions with damping function defined in Eq. (6). The PML layer thickness extends outwards 100 mm in both the radial and thickness directions from the endfaces of the fluid regions, indicated in Fig. 4 by the red colored regions. The mid frequency of the frequency range, $f_0 = 675$ kHz, has been used to get a frequency independent σ. The piston source is implemented with the center of the front surface in origo, indicated with a red box in Fig. 4. The steel plate is indicated in green in Fig. 4 with the "decreasing Q_M" method implemented from $r = 100$ mm to the endface of the steel plate. In this region the Q_M for the steel plate is exponentially reduced from 100 to 0.001. The water region above the piston source extends 50

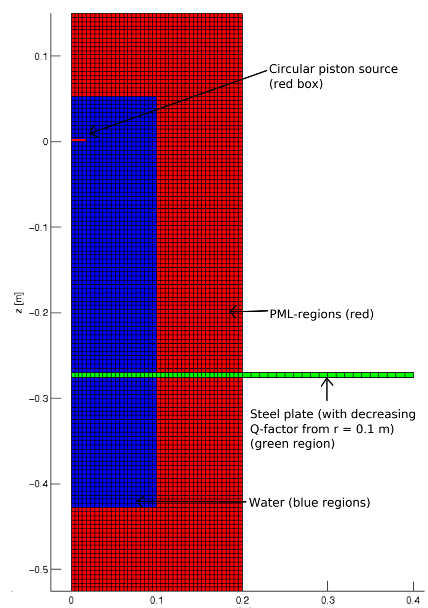

FIG 4. A decimated mesh of the axisymmetric FE simulation with PMLs (red regions) around the fluid regions (blue) and the steel plate (green region). PMLs extends outwards 100 mm in both directions from the endfaces of the regions, and the "decreasing Q_M" method begins in $r = 100$ mm. This coarse element division is used for illustration only, and is not used for the actual simulations.

mm in the z direction, and the water region below the steel plate extends 150 mm in the $-z$ direction. The frequency range of the simulations is from 350 kHz to 1 MHz, with 1 kHz step. 3 elements per compressional and shear wavelength at the maximum frequency of interest, $f_{max} = 1$ MHz, was used as the element division for the water and steel plate respectively. In the position along the plate where the PMLs are applied, the fluid PML element grid is in connection with the steel plate. This is in contradiction to [12] where a small gap is used, but for the setup used in this paper a connection between the fluid PML elements and the steel plate provides a better result. The time harmonic analysis [24] is used to calculate the pressure at all nodes in the water regions for each frequency of interest. The transmitted on-axis pressure $p^{\mathrm{FEM,sw}}$ is calculated at the on-axis node located nearest to the point at 100 mm below the lower surface of the steel plate, see '$*$' in Fig. 1. For all FE simulations the transmitted on-axis pressure $p^{\mathrm{FEM,sw}}$ is calculated at the on-axis node at 99.70356 mm below the lower surface of the steel plate.

5. Results

5.1. Leaky Lamb waves for an elastic plate (plane waves)

The plane wave pressure transmission coefficient T for the plate immersed in water using leaky Lamb wave theory is presented in Fig. 5. The figure shows the magnitude of the transmission coefficient $|T|$ for different incidence angles and for the frequency range of interest here. Maximum transmission coefficient $|T|$ corresponds to where the symmetrical and antisymmetrical Lamb modes, S_1, S_2, A_2 and A_3 (where S denotes symmetrical, A denotes antisymmetrical) are excited in the steel plate [4, 6]. As the angle of incidence approaches zero the symmetrical and antisymmetrical Lamb modes in the plate approach the critical frequencies, creating standing waves (TE and TS respectively) across the thickness of the steel plate, see Eqs. (1) and (2).

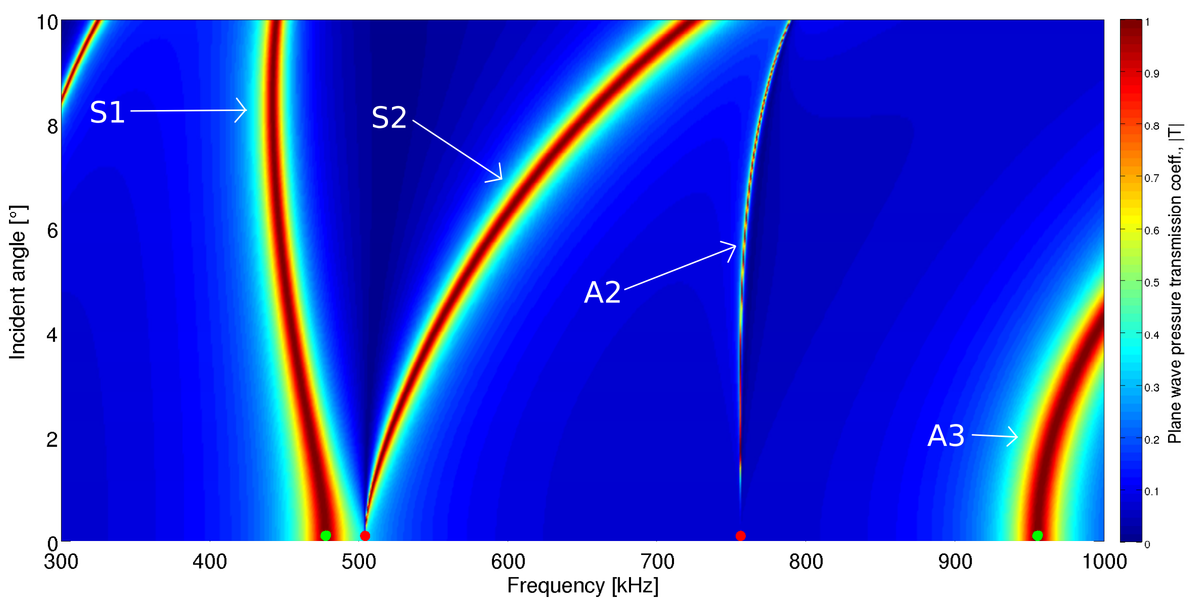

FIG 5. Magnitude of the pressure transmission coefficient, $|T|$, for leaky Lamb modes in a 6.05 mm steel plate with water loading [4]. A maximum pressure transmission coefficient $|T|$ corresponds to excitation of either the S_1, S_2, A_2 and A_3 mode in the plate. At normal incidence the S_1 and A_3 modes create thickness extensional (TE) modes across the thickness of the steel plate, which are marked with green dots. At normal incidene the TS modes are not excited, in terms of plane wave theory. At an incidence angle of 0.2° the S_2 and A_2 modes approach the thickness shear (TS) modes across the plate thickness, marked with red dots, [4].

As a plane wave with normal incidence to the plate only generates an extensional displacement in the plate, this plane wave will only excite compressional waves inside the plate. For that reason a plane wave at normal incidence cannot excite TS modes inside the plate, and the Lamb modes corresponding to these modes, the S_2 and the A_2 mode, will vanish as the incidence angle of the imposed plane wave approaches zero. The magnitude of the pressure transmission coefficient $|T|$ at normal incidence is presented in Fig. 6 as the black line [4, 6]. The frequencies where the $|T|$ has a maximum, corresponds to the frequencies of the S_1 and A_3 modes. At these frequencies, a standing TE mode will occur across the thickness of the steel plate. As the imposed plane wave has a normal incidence angle towards the plate no TS modes will be excited. Introducing a small incident angle of 1° the imposed plane wave will cause, in addition to an extensional displacement, a displacement in the radial direction of the plate. This radial displacement gives shear displacement which causes excitation of TS modes. The magnitude of the pressure transmission coefficient $|T|$ at 1° incidence angle is presented in the same figure as the blue line. Here the S_2 and A_2 mode will also be excited, causing a minima in $|T|$. The frequencies where these minima appear correspond approximately to the frequencies where TS modes are present across the thickness of the plate [4, 6]. No losses are included in the steel plate.

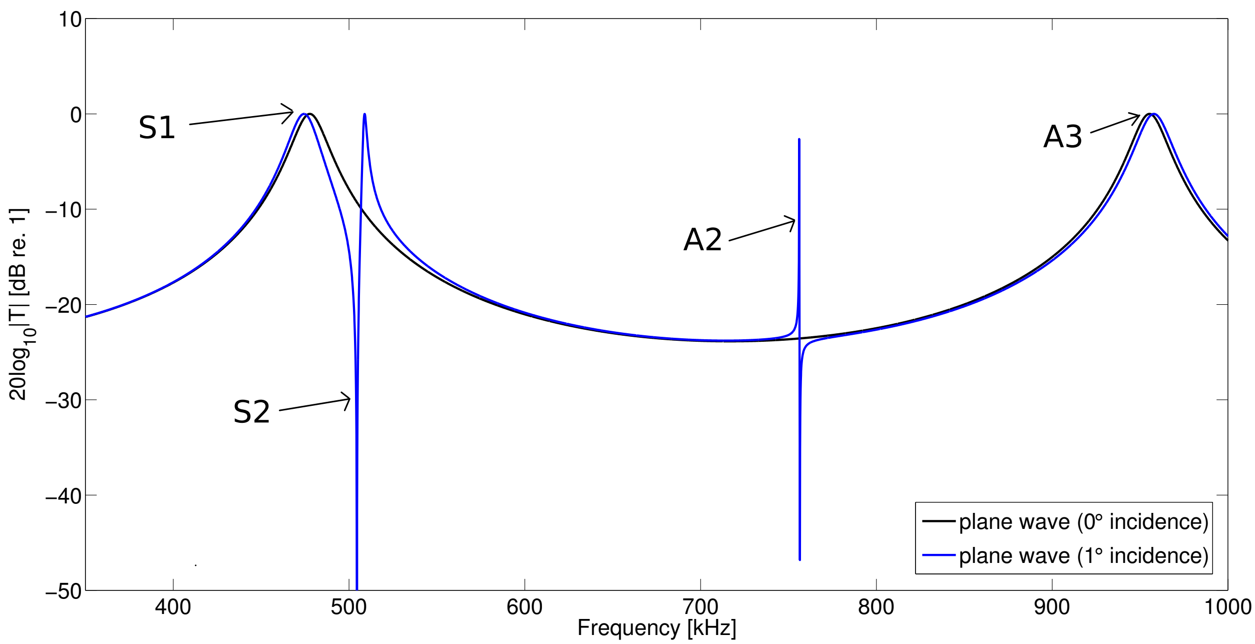

FIG 6. Magnitude of the pressure transmission coefficient $|T|$ at normal incidence and 1° angle of incidence (black and blue line respectively) using leaky Lamb wave theory [4, 6].

5.2. 3D Angular spectrum method (ASM)

In Fig. 7 the $\mathrm{TFS}_{inc}^{\mathrm{ASM}}$ is presented as the solid red line, together with the results from Fig. 6. Since the 3D ASM imposes a directive beam across the surface of the steel plate, displacements in both the thickness and radial direction will occur at normal incidence of the beam, since a beam contains a spectrum of plane waves with incidence angles from 0 to > 0. Both compressional and shear waves are thus set up in the plate, thereby exciting both TE and TS modes in the plate at normal incidence. There is a close agreement between the results using the 3D ASM and the plane wave theory for the frequencies where the magnitude of the pressure transmission coefficient $|T|$ and the $\mathrm{TFS}_{inc}^{\mathrm{ASM}}$ has maxima or minima, except around the S_1 mode. A shift downwards in frequency can here be experienced for the 3D ASM compared to the maximum calculated using the plane wave theory. One possible explanation may be that the beam excites both the S_1 and S_2 mode by various degree for the frequencies in that specific frequency range, since a beam contains a spectrum of plane waves with various incidence angles. Another possible explanation may be that using a beam causes the S_1 mode to shift downwards in frequency, recall that the S_1 mode in Fig. 5 shifts downwards in frequency when an incidence angle different from zero is introduced. Comparing the plane wave transmission coefficient $|T|$ (black and blue lines) to the $\mathrm{TFS}_{inc}^{\mathrm{ASM}}$ (red line) there exists a difference in magnitude of approximately 3 dB for frequencies away from the maxima and minima. Recall that the $\mathrm{TFS}_{inc}^{\mathrm{ASM}}$ is calculated from the transmitted on-axis pressure p^{ASM} at a distance of 100 mm from the lower surface of the plate, and the pressure transmission coefficient $|T|$ is calculated at the lower surface. If the pressure p^{ASM} is extrapolated to the lower surface of the plate, and since the pressure amplitude is inversely propotional to the range (a distance of 100 mm), an increase of the pressure p^{ASM} of approximately 3.16 dB will be experienced. A closer agreement for frequencies away from the Lamb modes for that case (red-dotted line) and the magnitude of the transmission coefficient $|T|$ can be observed in Fig. 7.

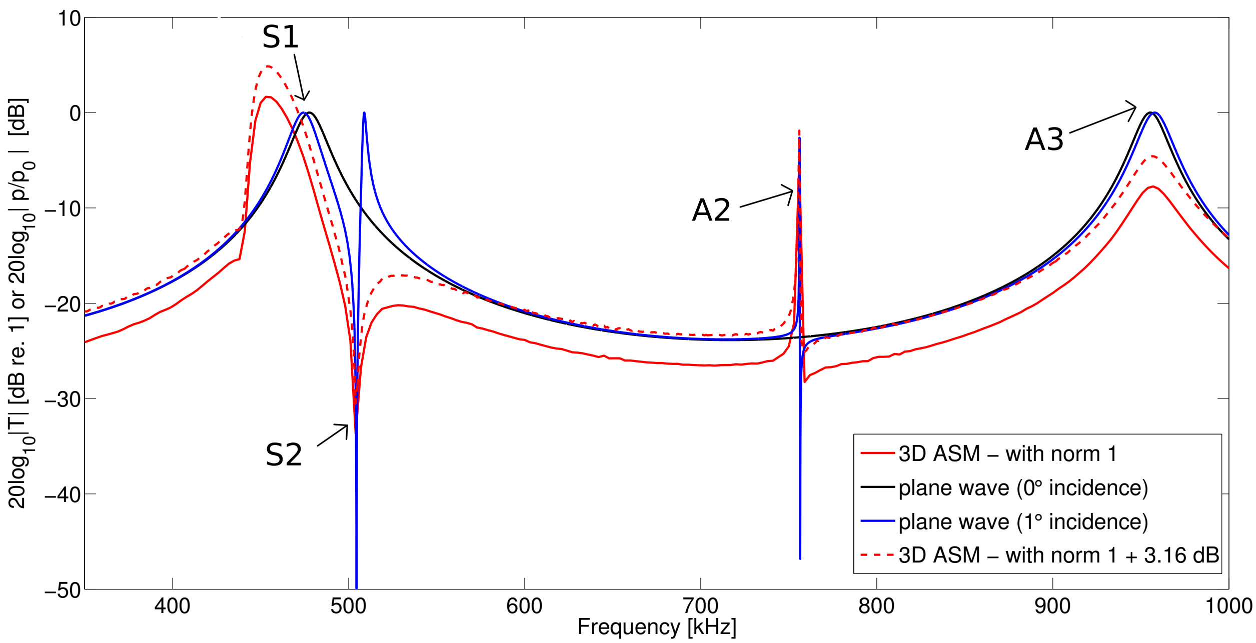

FIG 7. The TFS p/p_0 at normal incidence using the 3D ASM (red line) [4, 6] and the plane wave transmission coefficient T at normal incidence and 1° (black and blue line) using plane wave theory [4, 6]. The pressure p^{ASM} for the 3D ASM is calculated at 100 mm below the steel plate, and normalized to the incident pressure p_{inc}^{ASM} in the water at the upper surface of the steel plate when the plate is absent, i.e. using normalization method no. 1. The $\mathrm{TFS}_{inc}^{\mathrm{ASM}}$ with an increase of 3.16 dB is shown as the red-dotted line.

5.3. 3D Finite element method (FEM)

The 3D FEM uses an uniformly vibrating circular piston source immersed in water without any baffle. The far field directional factor $D(\theta)$ for the unbaffled piston at the upper surface of the steel plate when the plate is absent using the 3D FEM (blue line), at $z = -270$ mm, is presented in Fig. 8. This directional factor is compared to the far field directional factor at a distance of 1 m from a uniformly vibrating circular piston source mounted in a rigid baffle of infinite extent (red line), the source used in the 3D ASM. The far field directional factor $D(\theta)$ is calculated for four frequencies, 400 kHz, 500 kHz, 600 kHz, 700 kHz, presented in Fig. 8, in [6] the directional factor for the same frequencies are compared to measurements made by [4]. The rayleigh distance for the specific frequencies are 141 mm, 176.4 mm, 211.5 mm and 246.7 mm respectively. The directional factor $D(\theta)$ is normalized to the maximum pressure p_{max} at $z = -270$ mm and 1 m respectively.

Using the 3D FEM, the pressure field from the unbaffled circular piston source at 350 kHz has been calculated with and without the steel plate present, see Fig. 9(a) and Fig. 9(b) respectively. In Fig. 9(a) the outgoing pressure from the piston source used in the normalization method no. 1 is demonstrated. From the definition of the PMLs in Eq. (3) the PMLs will only dampen waves in one direction. Since the PMLs shall suppress outgoing waves in the radial direction for an axisymmetrical simulation the PMLs may not provide an accurate damping in relation to a full 3D solution where PMLs dampen reflections in the x, y and z directions respectively [26].

In Fig. 9(b) a standing wave pattern between the circular piston source and the steel plate can be observed. From such a simulation the transmitted on-axis pressure $p^{\mathrm{FEM,sw}}$ at a distance of 99.70356 mm below the lower surface of the steel plate is calculated. This pressure will be affected by the standing wave pattern created between the piston source and the steel plate. In order to reduce the effects this standing wave pattern will have on the transmitted frequency spectrum the normalization method no. 2 is used. The sound fields are shown in the fluid, to the start of the PML regions.

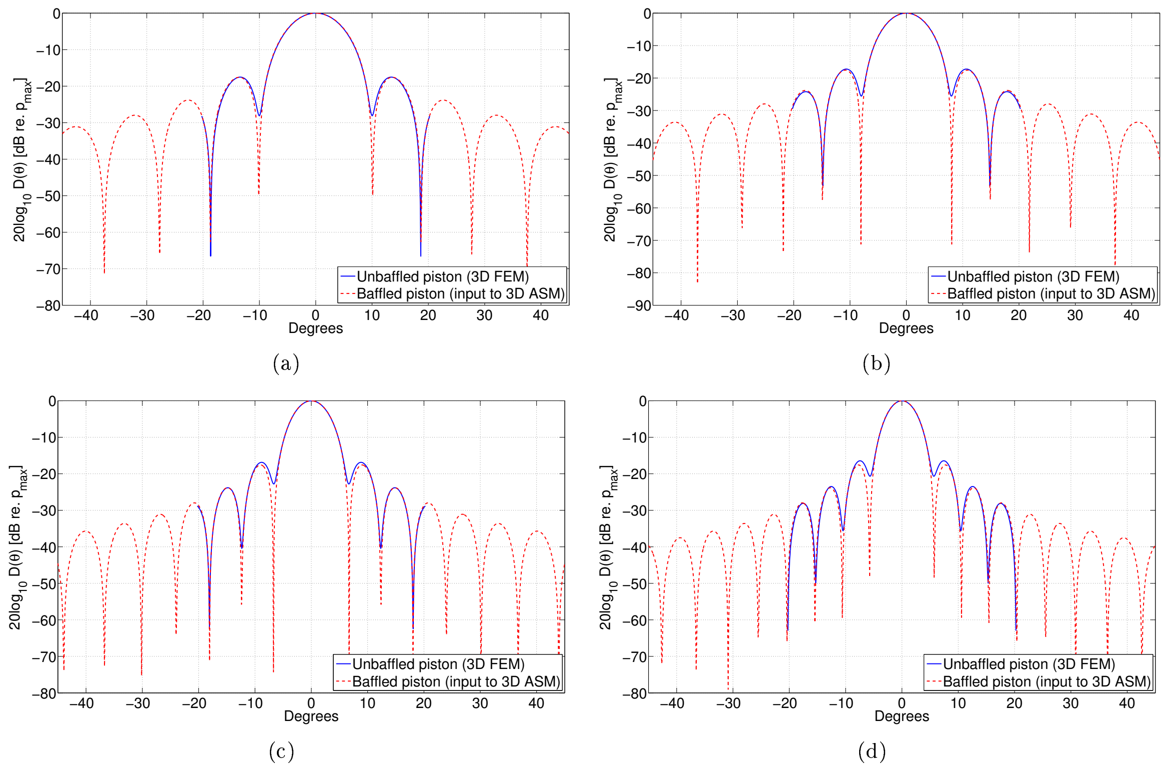

FIG 8. Far field directional factor $D(\theta)$ of the unbaffled piston calculated using 3D FEM (blue line) and the baffle piston model (red line)(used as input to the 3D ASM), respectively, at (a) 400 kHz and ka = 21.86, (b) 500 kHz and ka = 27.33, (c) 600 kHz and ka = 32.79, (d) 700 kHz and ka = 38.26. a = 12.9 mm. The rayleigh distance for the specific frequencies are 141 mm, 176.4 mm, 211.5 mm and 246.7 mm respectively.

The $\mathrm{TFS}_{inc}^{\mathrm{FEM,sw}}$ and $\mathrm{TFS}_{tot}^{\mathrm{FEM}}$ at normal incidence is presented in Fig. 10 in comparison with the $\mathrm{TFS}_{inc}^{\mathrm{ASM}}$ and $\mathrm{TFS}_{tot}^{\mathrm{ASM}}$. The $\mathrm{TFS}_{inc}^{\mathrm{FEM,sw}}$ oscillates approximately ± 8 dB around the $\mathrm{TFS}_{inc}^{\mathrm{ASM}}$, shown in Fig. 7, but the overall frequency dependencies of the spectra are very similar. p_{inc}^{FEM} does not include the effects of the standing waves, and therefore will these effects be present in the $\mathrm{TFS}_{inc}^{\mathrm{FEM,sw}}$, see Eq. (11). Calculating the $\mathrm{TFS}_{tot}^{\mathrm{FEM}}$ the oscillations present with normalization method no. 1 have almost vanished, and a closer agreement with the $\mathrm{TFS}_{tot}^{\mathrm{ASM}}$ can be observed. There is a small magnitude difference between the two methods, probably since the 3D FEM assumes a lossy steel plate where the 3D ASM does not. In addition there are small oscillations in the $\mathrm{TFS}_{tot}^{\mathrm{FEM}}$, possibly that the effects of the standing wave pattern are not entirely removed, or that there may exist small reflections from the endfaces of the fluid regions and/or the plate.

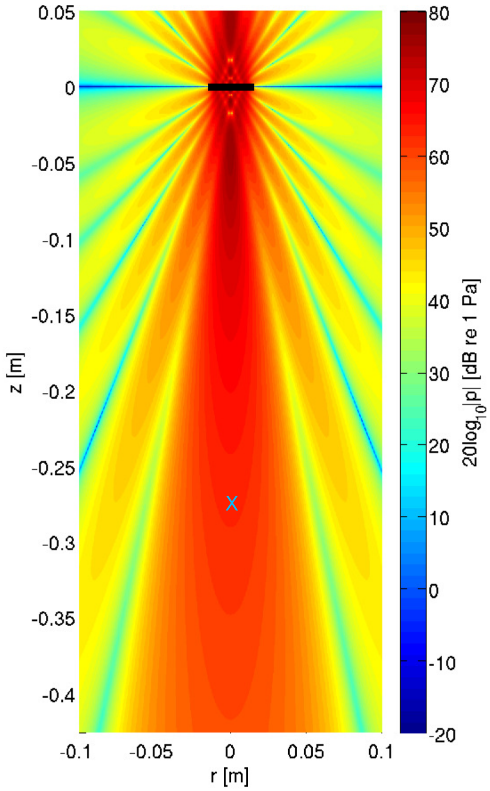

(a)

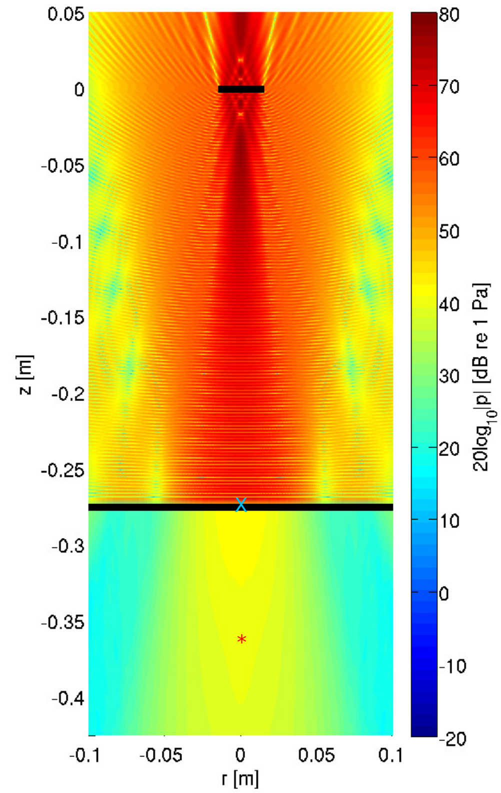

(b)

FIG 9. The pressure field from a circular piston source at 350 kHz simulated using finite elements. The piston source is indicated by the black rectangle at origo. The steel plate thickness is 6.05 mm. In Figs. 10 - 13 the transmitted on-axis pressure $p^{\mathrm{FEM,sw}}$ is calculated at '*', and the normalization on-axis pressure p_0 is calculated at 'X'. (a) The steel plate is absent. (b) The steel plate is present, indicated by the black rectangle at z = -270 mm.

Fig. 10 indicates that the normalization method no. 2 may be useful for calculating the transmitted frequency spectrum using the 3D FEM. Recall that the normalization method no. 2 uses the total on-axis pressure $p_{tot}^{\mathrm{FEM,sw}}$ in the water at the upper surface of the plate. The measurements made by [4, 6] uses the incident on-axis pressure p_{inc}^{MEAS} in the water at the upper surface of the plate to normalize the transmitted on-axis pressure p^{MEAS} (normalization method no. 1). In order to compare the $\mathrm{TFS}_{tot}^{\mathrm{FEM}}$ to the measurements made by [4, 6] the relationship between the two normalization methods must be calculated.

The $\mathrm{TFS}_{inc}^{\mathrm{ASM}}$ may be expressed as

$$\mathrm{TFS}_{inc}^{\mathrm{ASM}} = \frac{p^{\mathrm{ASM}}}{p_{inc}^{\mathrm{ASM}}} = \frac{p^{\mathrm{ASM}}}{p_{tot}^{\mathrm{ASM}}}\frac{p_{tot}^{\mathrm{ASM}}}{p_{inc}^{\mathrm{ASM}}}. \tag{13}$$

which can be expressed using Eq. (10) as

$$\mathrm{TFS}_{inc}^{\mathrm{ASM}} = \mathrm{TFS}_{tot}^{\mathrm{ASM}}\frac{p_{tot}^{\mathrm{ASM}}}{p_{inc}^{\mathrm{ASM}}}, \tag{14}$$

where $p_{tot}^{\mathrm{ASM}}/p_{inc}^{\mathrm{ASM}}$ gives the ratio between the TFS for the two normalization methods in the 3D ASM.

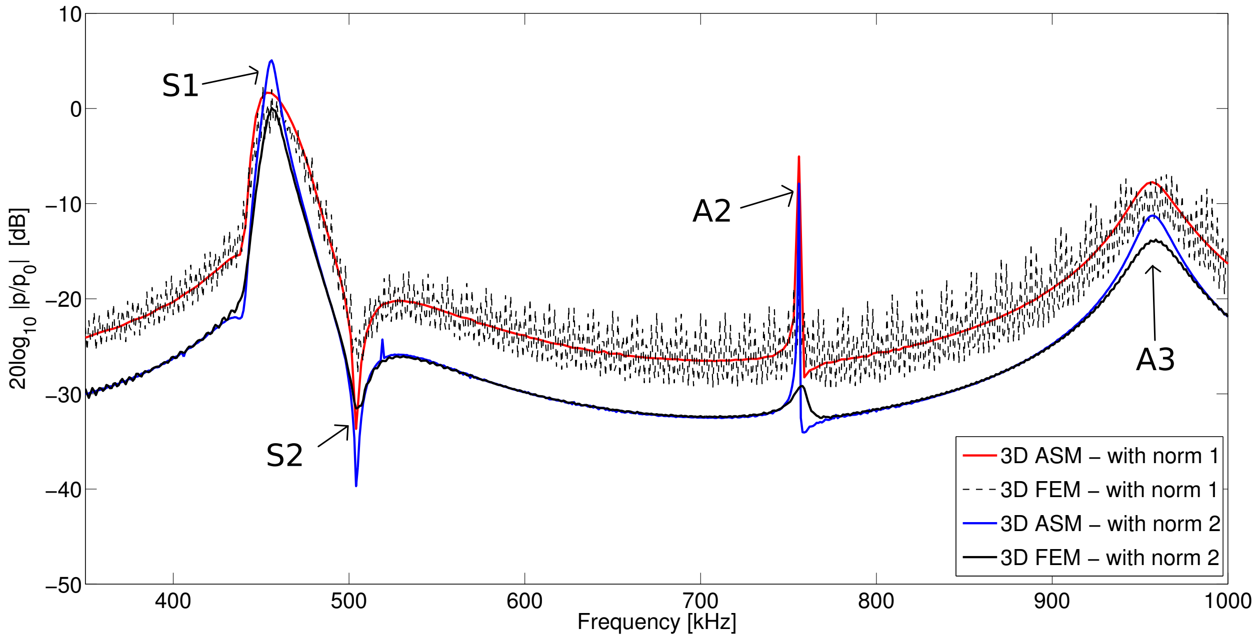

FIG 10. Transmitted frequency spectra at normal incidence using the 3D ASM and 3D FEM. Transmitted on-axis pressure calculated at 100 mm below the steel plate for the 3D ASM, and 99.70356 mm for the 3D FEM. The transmitted pressure p calculated using the 3D FEM and the 3D ASM are normalized with both normalization methods.

The same can be expressed for the $\mathrm{TFS}_{inc}^{\mathrm{FEM,sw}}$ as

$$\mathrm{TFS}_{inc}^{\mathrm{FEM,sw}} = \frac{p^{\mathrm{FEM,sw}}}{p_{inc}^{\mathrm{FEM}}} = \frac{p^{\mathrm{FEM,sw}}}{p_{tot}^{\mathrm{FEM,sw}}} \frac{p_{tot}^{\mathrm{FEM,sw}}}{p_{inc}^{\mathrm{FEM}}}, \tag{15}$$

which can be expressed using Eq. (11) as

$$\mathrm{TFS}_{inc}^{\mathrm{FEM,sw}} = \mathrm{TFS}_{tot}^{\mathrm{FEM}} \frac{p_{tot}^{\mathrm{FEM,sw}}}{p_{inc}^{\mathrm{FEM}}}, \tag{16}$$

where $p_{tot}^{\mathrm{FEM,sw}}/p_{inc}^{\mathrm{FEM}}$ gives the ratio between the TFS for the two normalization methods in the 3D FEM.

If the elastic steel plate were a rigid plate, excluding internal wave propagation, the ratio $p_{tot}/p_{inc} = 2$, i.e. a 6 dB difference between the two normalization methods. From Fig. 10 a difference in magnitude of approximately 6 dB can be observed between the normalization methods, exept around the Lamb modes of the steel plate. However, as the plate is not rigid, but supports elastic waves, one may expect deviations from such a simplified rigid-plate consideration, especially around the Lamb modes of the plate.

A more refined method for calculating the ratio p_{tot}/p_{inc} has been used. The perferable choice would be to calculate this ratio using the 3D FEM. However, since p_{inc}^{FEM} cannot include the standing wave pattern that will be present in $p_{tot}^{\mathrm{FEM,sw}}$, the effects of the standing wave pattern cannot be removed from that ratio, and will be present in the $\mathrm{TFS}_{inc}^{\mathrm{FEM,sw}}$, see Eq. (16). Instead, the ratio has been approximated by using the 3D ASM [4, 6] with a lossy steel plate with a $Q_M = 100$. The ratio will then include the effects the plate will have on the total on-axis pressure p_{tot}^{ASM}, but not the effects of the standing wave pattern present in $p_{tot}^{\mathrm{FEM,sw}}$. Fig. 11 presents the ratio between the normalization method no. 2 and the normalization method no. 1, $p_{tot}^{\mathrm{ASM}}/p_{inc}^{\mathrm{ASM}}$, see Eq. (14). Away from the Lamb modes an approximate 6 dB difference between the two normalization methods is observed. Around the Lamb modes the ratio becomes smaller, probarly due to resonance effects, see Fig. 5 where the plane wave transmission coefficient $|T|$ has maxima in near proximity of the different symmetrical Lamb modes. If this ratio (Fig. 11) is added to the $\text{TFS}_{tot}^{\text{FEM}}$ (blue line) (Fig. 10) a closer agreement to the $\text{TFS}_{inc}^{\text{ASM}}$ (red line) can be observed, see Fig. 12, except around the Lamb modes, possibly because the 3D ASM does not include losses in the steel plate.

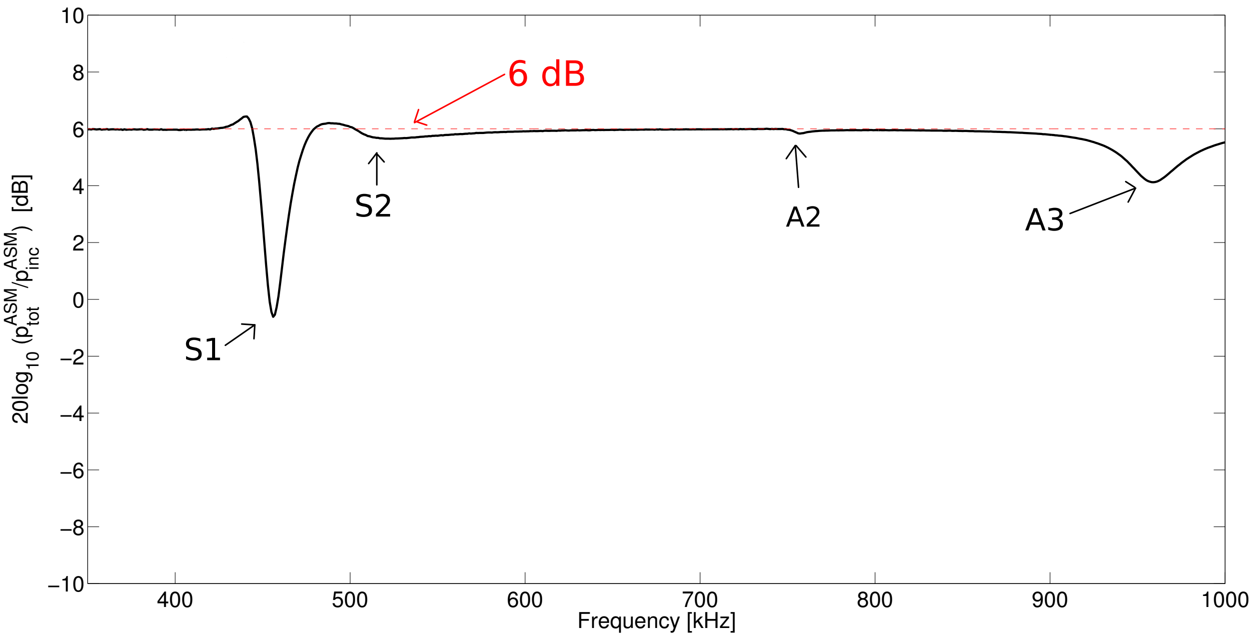

FIG 11. The ratio between the total (incident + reflected) on-axis pressure p_{tot}^{ASM} (norm no. 2) when the plate is present to the incident on-axis pressure p_{inc}^{ASM} (norm no. 1) when the plate is absent using the 3D ASM [4]. A lossy steel plate with a $Q_M = 100$ is assumed for the 3D ASM.

From the measurements on the steel plate, described in Section 3, a new shear velocity of $c_S = 3130$ m/s was determined [4]. In order to compare the simulation results to the measurements, simulations with a new shear velocity of the steel plate are calculated. In Fig. 13 a comparison of the simulated (3D ASM and 3D FEM) and measured (black line) transmitted frequency spectra are presented, the $\text{TFS}_{inc}^{\text{ASM}}$ (red line) and the $\text{TFS}_{tot}^{\text{FEM}}$ (blue line) with a ratio similar to Fig. 11 included (the ratio for the simulation corresponds to Fig. 11 with $c_S = 3130$ m/s, not shown here). This figure demonstrates a relative close agreement between both methods and the measurements, but the same magnitude differences present in Fig. 12 between the 3D FEM and 3D ASM around the Lamb modes are still present. The $\text{TFS}_{inc}^{\text{MEAS}}$ is limited to the frequency range of 350 kHz to 800 kHz. The magnitude difference at the S_1 mode indicates that the $Q_M = 100$ for the steel plate in the 3D FEM is to low, and possibly a higher Q_M would provide a closer agreement with measurements.

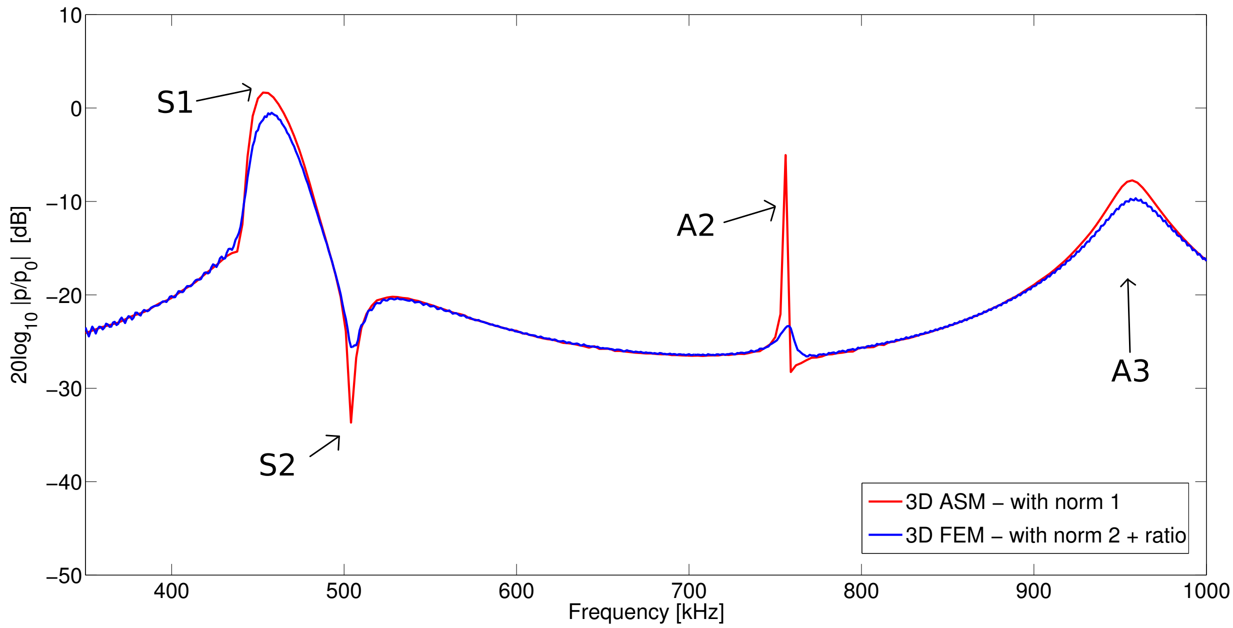

FIG 12. TFS at normal incidence for the 3D ASM with normalization method no.1 (red line), and the 3D FEM (norm 2), corrected using $p_{tot}^{\mathrm{ASM}}/p_{inc}^{\mathrm{ASM}}$ from Fig. 11 (blue line). The transmitted on-axis pressure is calculated at 100 mm below the steel plate for the 3D ASM, and at a distance of 99.70356 mm for the 3D FEM.

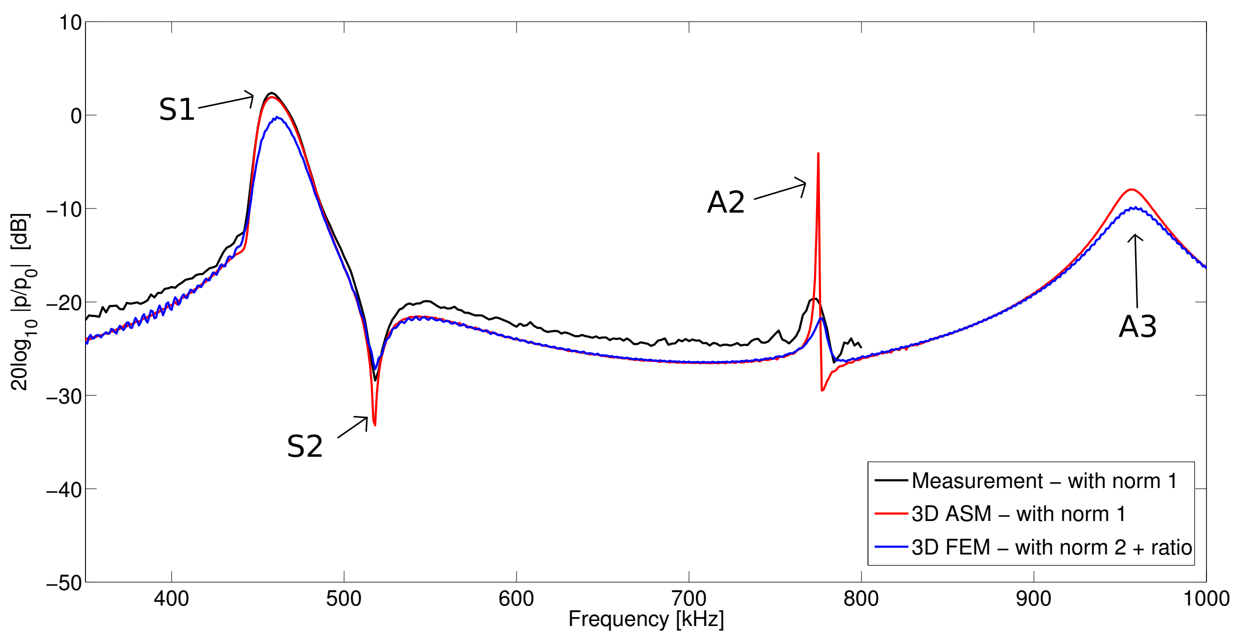

FIG 13. TFS at normal incidence for the 3D ASM (red line) and the 3D FEM (blue line) in comparison with the spectrum measured by [4, 6]. The transmitted on-axis pressure is calculated at 100 mm below the steel plate for the 3D ASM, and at a distance of 99.70356 mm for the 3D FEM. The transmitted on-axis pressure calculated using the 3D FEM is normalized with method no. 2 and with a ratio similar to Fig. 11 included. The 3D ASM is normalized using normalization method no. 1.

5.4. Critical frequencies

In [4] a measurement method for determing the sound compressional and shear velocity of an elastic steel plate is discussed. The discussion is based on the plane wave pressure transmission T and $\mathrm{TFS}_{inc}^{\mathrm{ASM}}$, with emphasis on which Lamb modes that could be used in such a method. It is of interest to investigate how this approach would relate to the use of the FEM.

Here, the $\mathrm{TFS}_{tot}^{\mathrm{FEM}}$ is compared to the results in [4]. From the plane wave theory presented in Section 2.1, standing compressional (TE) and shear (TS) waves will be present across the thickness of a plate for certain frequencies. At these frequencies the compressional and shear velocity can be calculated from Eqs. (1) and (2) respectively, see Section 2.1 and [4].

The critical frequencies in Eq. (1) correspond to the frequencies where the magnitude of the plane wave transmission coefficient $|T|$ in Fig. 6 at normal incidence (black line) has a maximum. Since a plane wave at normal incidence only generates an extensional displacement, a plane wave with an 1° incidence angle, see Fig. 6 (blue line), is used to approximate the critical frequencies in Eq. (2) where the magnitude of the plane wave transmission coefficient $|T|$ has a minimum. These frequencies are given in Table 2.

In Fig. 7 the frequencies where the $\mathrm{TFS}_{inc}^{\mathrm{ASM}}$ has a maximum or a minimum can be determined. These are presented in the third column in Table. 2. There is a close agreement between these frequencies and the ones determined from Fig. 6, exept for the frequency corresponding to the S_1 mode, as expected from the deviations in Fig. 7 between the $\mathrm{TFS}_{inc}^{\mathrm{ASM}}$ and the plane wave theory at normal incidence.

In Fig. 10 the frequencies where the $\mathrm{TFS}_{tot}^{\mathrm{FEM}}$ has a maximum or a minimum can be determined. These are presented in the fourth column in Table 2. Comparing these frequencies to the frequencies determined from the $\mathrm{TFS}_{inc}^{\mathrm{ASM}}$ there is a relative close agreement for all four frequencies.

TABLE 2. Frequencies corresponding to a maximum or a minimum for the magnitude of the plane wave transmission coefficient $|T|$ [4]. Frequencies corresponding to a maximum or a minimum of the $\mathrm{TFS}_{inc}^{\mathrm{ASM}}$ [4] and the $\mathrm{TFS}_{tot}^{\mathrm{FEM}}$. The * indicates a 1° incidence angle with the steel plate. (w.t – wave theory)

	Leaky Lamb w.t, Fig. 6	$\mathrm{TFS}_{inc}^{\mathrm{ASM}}$, Fig. 7	$\mathrm{TFS}_{tot}^{\mathrm{FEM}}$, Fig. 10
$f_{L,1}$ [kHz]	477.7	454.5	457.7
$f_{S,2}$ [kHz]	504.5*	504.2	506.2
$f_{S,3}$ [kHz]	756.5*	755.9	759.9
$f_{L,2}$ [kHz]	955.4	956.7	957.4

The frequencies in Table 2 have been used to calculate the compressional and shear velocities of the steel plate using Eqs. (1) and (2) respectively, for each model. The calculated sound velocities of the steel plate are given in Table 3 for each model, determined at each frequency given in Table 2. A comparison between the plane wave results and the input simulation parameters, $c_L = 5780$ m/s and $c_S = 3050$ m/s (see Table 1), demonstrates a close agreement for all four frequencies.

The frequencies in Table 2 for the $\mathrm{TFS}_{inc}^{\mathrm{ASM}}$ and the $\mathrm{TFS}_{tot}^{\mathrm{FEM}}$ are used to calculate the sound velocities in the steel plate using the same equations as for the plane wave, Eqs. (1) and (2). The determined sound velocity is presented in the third and fourth column of Table 3 respectively. A comparison with the material data for the steel plate illustrates a relative close agreement for the sound velocities calculated from the frequencies in Table 2, exept for the compressional velocity determined at the frequency corresponding to the S_1 mode. This indicates that the S_1 mode may not be used for determining the compressional velocity in the steel plate for a real directive beam, but that using the S_2, A_2 and A_3 mode may provide a reasonable estimate of the sound velocities.

TABLE 3. Calculated sound velocities using Eqs. (1) and (2) with the frequencies listed in Table 2. The * indicates a 1° incidence angle with the steel plate.

	Leaky Lamb wave theory	$\text{TFS}_{inc}^{\text{ASM}}$	$\text{TFS}_{tot}^{\text{FEM}}$
$c_{L,1}$ [m/s]	5780.17	5499.45	5538.17
$c_{S,2}$ [m/s]	3052.23*	3050.41	3062.51
$c_{S,3}$ [m/s]	3051.22*	3048.79	3064.93
$c_{L,2}$ [m/s]	5780.17	5788.04	5792.27

6. Conclusions

3D FEM has been applied to study the interaction of an acoustic beam with an elastic steel plate at normal incidence. Due to the normal incidence and the frequency domain 3D FEM, a standing wave pattern between the piston source and the steel plate is present in the FE simulations. Since the transmitted on-axis pressure is affected by this, a normalization method is employed, which attempts to remove these effects. In order to compare the 3D FEM with the 3D ASM and measurements, a relationship between this normalization method and the one used for the 3D ASM and the measurements is presented. The relationship has been derived using the 3D ASM, and the 3D FEM using this relationship has been successfully compared to the 3D ASM and measurements. There are still small deviations in the TFS, possibly due to the losses included in the 3D FEM. The transmitted frequency spectrum of the beam using the 3D FEM has also been successfully compared to the results in [4], for the proposed method for determining the compressional and shear sound velocity in the steel plate.

Acknowledgements

This work has been supported through the 4 year Ph.D. project: ”Full wave propagation of acoustic beams in viscoelastic media; finite element modeling and measurements”, financed by the University of Bergen. The work is supervised by Per Lunde and Magne Vestrheim, in a cooperation with the Department of Earth Science at the University of Bergen and the Michelsen Centre for Industrial Measurement Science and Technology.

References

[1] M. Sanderson and H. Yeung, “Guidelines for the use of ultrasonic non-invasive metering techniques”, Flow Measurement and Instrumentation **13**, 125–142 (2002).

[2] P. Lunde, K. Frøysa, and M. Vestrheim, *GERG project on ultrasonic gas flow meters, Phase 2*, VDI Verlag, Düsseldorf, 2000.

[3] M. Drozdz, “Efficient Finite Element Modelling Of Ultrasound Waves in Elastic Media”, Ph.D. thesis, Imperial College, London (2008).

[4] K. D. Lohne, “”', Ph.D. thesis, University of Bergen, Department of Physics and Technology, Bergen, Norway [in progress].

[5] K. D. Lohne, M. Vestrheim, and P. Lunde, “Study of a steel plate immersed in water”, in *Proceedings of the 31st Scandinavian Symposium on Physical Acoustics* (Geilo, Norway) (2008).

[6] K. D. Lohne, P. Lunde, and M. Vestrheim, “Measurements and 3D simulations of ultrasonic directive beam transmission through a water-immersed steel plate”, in *Proceedings of the 34th Scandinavian Symposium on Physical Acoustics* (Geilo, Norway) (2011).

[7] D. N. Alleyne, “The non-destructive testing of plates using ultrasonic Lamb waves”, Ph.D. thesis, Imperial College, London (1991).

[8] M. Lowe, "Matrix techniques for modeling ultrasonic waves in multilayered media", IEEE Transactions on Ultrasonics, Ferroelectrics and Frequency Control, **42**(4), 525–542 (1995).

[9] M. J. S. Lowe, "Plate waves for the NDT of diffusion bonded titanium", Ph.D. thesis, Imperial College, London (1992).

[10] S. J. Younghouse, "Irradiation of an elastic plate by a finite-amplitude sound beam with applications to nondestructive evaluation", Ph.D. thesis, University of Austin, Texas (2002).

[11] B. J. Landsberger and M. F. Hamilton, "Second-harmonic generation in sound beams reflected from, and transmitted through, immersed elastic solids", Journal of the Acoustical Society of America **109**(2), 488–500 (2001).

[12] R. A. Kippersund, J. Kocbach, and P. Lunde, "Simulation of guided waves in a fluid loaded elastic plate", in *Proc. of 31st Scandinavian Symposium on Physical Acoustics* (Geilo, Norway) (2008).

[13] R. Kippersund, P. Lunde, and K. Frøysa, "Deposit detection using plate waves", in *Proceedings of the 32nd Scandinavian Symposium on Physical Acoustics* (Geilo, Norway) (2009).

[14] R. Kippersund, P. Lunde, and K. Frøysa, "Measurement of fluid viscosity in pipes using multimode ultrasonic guided wave attenuation", in *Proceedings of Baltic-Nordic Acoustic Meeting 2010* (Bergen, Norway) (2010).

[15] J. Kocbach, R. A. Kippersund, and P. Lunde, "Time Domain Finite Element Modeling of SH-mode propagation in elastic plates with deposits", in *Proceedings of the 33rd Scandinavian Symposium on Physical Acoustics* (Geilo, Norway) (2010).

[16] A. Schoch, "Der schalldurchgang durch platten", Acustica **2**(1), 1–17 (1952).

[17] R. Fiorito and H. Uberall, "Resonance theory of acoustic reflection and transmission through a fluid layer", Journal of the Acoustical Society of America **65**(1), 9–14 (1979).

[18] R. Fiorito, W. Madigosky, and H. Uberall, "Resonance theory of acoustic waves interacting with an elastic plate", Journal of the Acoustical Society of America **66**(6), 1857–1866 (1979).

[19] H. Bertoni and T. Tamir, "Unified theory of Rayleigh-angle phenomena for acoustic beams at liquid-solid interfaces", Applied Physics A: Materials Science & Processing **2**(4), 157–172 (1973).

[20] T. J. Plona, L. E. Pitts, and W. G. Mayer, "Ultrasonic bounded beam reflection and transmission effects at a liquid/ solid-plate/liquid interface", Journal of the Acoustical Society of America **59**(6), 1324–1328 (1976).

[21] L. Pitts, T. Plona, and W. Mayer, "Theory of Nonspecular Reflection. Effects for an Ultrasonic Beam Incident on a Solid Plate in a Liquid", IEEE Transactions on Sonics and Ultrasonics **24**(2), 101–108 (1977).

[22] I. A. Viktorov, *Rayleigh and Lamb waves. Physical theory and applications* (Plenum Press, New York, USA) (1967).

[23] J. Rose, *Ultrasonic waves in solid media* (Cambridge University Press, U.K.) (1999).

[24] J. Kocbach, "Finite Element Modeling of Ultrasonic Piezoelectric Transducers", Ph.D. thesis, Department of Physics and Technology, University of Bergen, Norway (2000).

[25] J. Kocbach, P. Lunde, and M. Vestrheim, "Resonance Frequency Spectra with Convergence Tests of Piezoceramic Disks using the Finite Element Method", Acta Acustica united with Acustica **87**, 271–285 (2001).

[26] J. Kocbach, P. Lunde, M. Vestrheim, and R. A. Kippersund, “Finite element modeling of ultrasonic piezoelectric transducers. Extension of FEMP to 3D analysis”, (2006).

[27] J.-P. Berenger, “A perfectly matched layer for the absorption of electromagnetic waves”, Journal of Computational Physics **114**(2), 185–200 (1994).

[28] A. Bermúdez, L. Hervella-Nieto, A. Prieto, and R. Rodriguez, “An optimal perfectly matched layer with unbounded absorbing function for time-harmonic acoustic scattering problems”, Journal of Computational Physics **223**(2), 469–488 (2007).

[29] M. Kaltenbacher and R. Lerch, “Perfectly Matched Layer Technique for the Numerical Computation of Wave Propagation Phenomena”, IEEE Ultrasonics Symposium Proceedings , 183–186 (2007).